In Vivo Melanoma Cell Morphology Reflects Molecular Signature and Tumor Aggressiveness

JID Open

Alessandra Marconi[1,7], Marika Quadri[1,7], Francesca Farnetani[2], Silvana Ciardo[2], Elisabetta Palazzo[1], Roberta Lotti[1], Anna Maria Cesinaro[3], Luca Fabbiani[4], Cristina Vaschieri[1], Mario Puviani[5], Cristina Magnoni[2], Shaniko Kaleci[2], Carlo Pincelli[1] and Giovanni Pellacani[2,6]

Melanoma is the deadliest type of skin cancer characterized by high cellular heterogeneity, which contributes to therapy resistance and unpredictable disease outcome. Recently, by correlating reflectance confocal microscopy morphology with histopathological type, we identified four distinct melanoma subtypes: dendritic cell, round cell, dermal nest, and combined-type melanomas. In this study, each reflectance confocal microscopy melanoma subtype expressed a specific biomolecular profile and biological behavior in vitro. Markers of tumor aggressiveness, including Ki-67, MERTK, nestin, and stemness markers were highest in the most invasive combined-type and dermal nest melanomas than in dendritic cell and round cell melanomas. This was also confirmed in multicellular tumor spheroids. Transcriptomic analysis showed modulation of cancer progression-associated genes from dendritic cell to combined-type melanomas. The switch from E- to N-cadherin expression proved the epithelial-to-mesenchymal transition from dendritic cell to combined-type subtypes. The dermal nest melanoma was predominantly located in the dermis, as also shown in skin reconstructs. It displayed a unique behavior and a molecular profile associated with a high degree of aggressiveness. Altogether, our results show that each reflectance confocal microscopy melanoma subtype has a distinct biological and gene expression profile related to tumor aggressiveness, confirming that reflectance confocal microscopy can be a dependable tool for in vivo detection of different types of melanoma and for early diagnostic screening.

Journal of Investigative Dermatology (2022) **142,** 2205–2216; doi:10.1016/j.jid.2021.12.024

INTRODUCTION

Melanoma is an extremely aggressive skin cancer consisting of several cell populations that show diverse genotypic and phenotypic features, signaling pathways, biological behavior, and response to therapy, suggesting the existence of a heterogeneous family of diseases rather than a unique entity (Scolyer et al., 2011). Melanoma is characterized by high metastatic capacity and resistance to conventional chemotherapy and in part to new targeted drugs (Jenkins and Fisher, 2021; Wilson and Schuchter, 2016).

Given its threatening potential, early detection remains the key factor in lowering melanoma-associated mortality. Classification is important for tumor diagnosis and prognosis. Melanoma is currently classified on the basis of different parameters such as histopathological type, vertical growth, and spreading to nearby lymph nodes or to any other organs (Gershenwald et al., 2017). However, it has become clear that this classification and staging system fails to account for different progression models of melanoma and to preselect patients for a specific treatment (Viros et al., 2008). This implies the need for new criteria and methodology to classify melanoma.

Reflectance confocal microscopy (RCM) is an emerging technology for the noninvasive analysis of skin tissue in real-time and at near-histopathological resolution (Fink and Haenssle, 2017). Recently, we proposed the existence of four distinct melanoma subtypes on the basis of the correlation between RCM-observed cell morphology and histopathological/patients' clinical features: (i) dendritic cell (DC) melanoma, with a predominant population of melanoma cells with a dendritic shape in the epidermal layer; (ii) round cell (RC) melanoma, mostly composed of large roundish cell population in the epidermal layer and at the dermal–epidermal junction; (iii) dermal nest (DN) melanoma, characterized by the presence of a dermal cerebriform nesting; and (iv) combined-type (CT) melanoma, which shows a combination of all the three confocal patterns (Pellacani

[1]*DermoLAB, Department of Surgical, Medical, Dental and Morphological Science, University of Modena and Reggio Emilia, Modena, Italy;* [2]*Dermatology Unit, Department of Surgical, Medical, Dental and Morphological Sciences, University of Modena and Reggio Emilia, Modena, Italy;* [3]*Department of Pathology, Azienda Ospedaliero-Universitaria Policlinico, University of Modena and Reggio Emilia, Modena, Italy;* [4]*Department of Medical and Surgical Sciences, University of Modena and Reggio Emilia, Modena, Italy;* [5]*Unit of Dermatology and Surgical Dermatology, Sassuolo Hospital, Sassuolo, Modena, Italy; and* [6]*Dermatology Clinic, Department of Clinical, Internal Medicine, Anesthesiology and Cardiovascular Sciences, Sapienza University of Rome, Rome, Italy*

[7]*These authors contributed equally to this work.*

Correspondence: Alessandra Marconi, DermoLAB, Department of Surgical, Medical, Dental and Morphological Science, University of Modena and Reggio Emilia, via Del Pozzo, 71 41124 - Modena, Italy. E-mail: alessandra.marconi@unimore.it

Abbreviations: BI, Breslow index; BP, biological process; CT, combined-type; DC, dendritic cell; DN, dermal nest; ECM, extracellular matrix; GO, Gene Ontology; RC, round cell; RCM, reflectance confocal microscopy

Received 19 May 2021; revised 29 November 2021; accepted 6 December 2021; accepted manuscript published online 7 January 2022; corrected proof published online 1 February 2022

et al., 2014). Previous work showed a correlation between patients' features and melanoma subtypes, suggesting that RCM cell morphology may be associated with different tumor stages and biological behavior (Grazziotin et al., 2016). Accordingly, a biological heterogeneity among RCM subtypes based on the different expression of tumor-associated biomarkers was recently shown (Beretti et al., 2019).

Specific genetic alterations are associated with precise clinical and histopathological features of melanoma, indicating that they may be helpful in refining existing disease classification (Whiteman et al., 2011). Yet, the existence of a close correlation among RCM melanoma subtypes, genetic signature, and biological behavior remains to be clarified.

In this work, we detected significant modifications in the expression of specific melanoma biomarkers in the RCM subtypes, and we present evidence that the four melanoma groups display different genetic profiles and biological behavior in vitro, which closely correlate with tumor aggressiveness.

RESULTS

RCM subtypes reflect patient/tumor characteristics

A total of 90 patients with a median age of 60.9 years were analyzed in this study. Representative clinical, histopathological, and RCM images are illustrated in Supplementary Figure S1. DC melanomas were mainly classified as melanoma in situ (44%) or radial growth phase type (48%) with a Breslow index (BI) less than 1 mm and a mitotic index between 0 and 1 (Table 1).

Given that it is the most frequent alteration in melanoma (Inumaru et al., 2014), only the $BRAF^{V600E}$ mutational status was evaluated in RCM melanoma subtypes. Interestingly, DC presented significantly fewer $BRAF^{V600E}$ mutations than the other RCM subtypes (Table 1).

RC melanoma was thicker than DC melanoma, as showed by the mean BI (0.6 vs. 0.2 mm, respectively). RC melanomas were either of the radial growth phase or vertical growth phase type (56% and 44%, respectively), despite their low mitotic index (96% between 0 and 1). Interestingly, none of the RC melanoma types was classified as melanoma in situ. CT and DN melanomas were mostly of the vertical growth phase type (96% and 93%, respectively), showing a high mitotic index (40% between 2 and 4 mm). Moreover, DN melanomas were significantly thicker than the other RCM types, with a mean BI of 5.8 mm.

By observing patients' history, 36% of patients with DC type had a previous history of melanoma, mainly melanoma in situ (data not shown), and 40% of them developed new melanomas, compared with the other RCM subtypes (Table 1). However, none of the DC types progressed to metastasis. On the contrary, CT and DN types significantly tended to metastasize, as revealed by the percentage of positive sentinel lymph nodes (32% and 27%, respectively) and metastases at 0–5 years (20% and 34%, respectively) (Table 1).

RCM morphology correlates with aggressiveness, stemness markers expression, and biological behavior in vitro

To analyze the growth fraction in each RCM subtype, the expression of Ki-67 proliferation marker was evaluated both in the epidermis and dermis (Figure 1a). In DC melanomas, Ki-67 was exclusively expressed in the epidermis, whereas DN melanomas expressed the marker only in the dermis. The expression of Ki-67 in RC melanoma was mainly localized in the epidermis, with a fraction of positive cells in the dermis. Conversely, CT melanoma expressed elevated levels of Ki-67 both in the epidermis and dermis.

MERTK and the intermediate filament nestin are associated with melanoma aggressiveness and progression (Schlegel et al., 2013). The expression of these markers significantly increased from DC to CT and DN melanomas, whereas no differences were observed between CT and DN melanomas (Figure 1a). The expression of HIF1α, which is known to stimulate angiogenesis (Widmer et al., 2013), was significantly higher in RC than in CT and DN melanomas. Moreover, the expression of SOX-10, known to affect melanoma cell proliferation, survival, and invasion (Graf et al., 2014), significantly increased from DC to CT and DN melanomas (Figure 1a).

The melanoma-initiating cells, which significantly contributes to the initiation, metastasis, and recurrence of melanoma, consist of a cell subpopulation expressing various markers such as the ABCB5 (Schatton et al., 2008), CD133 (Monzani et al., 2007), SOX-2 (Santini et al., 2014), and CD271 (Boiko et al., 2010). ABCB5 expression significantly increased from DC to CT and DN melanomas, whereas no differences were found between CT and DN melanomas. On the contrary, SOX-2 and CD133 were significantly more expressed in DN melanoma. Although it is considered a melanoma-initiating cells marker, CD271 downregulation has been shown to promote melanoma progression and invasion (Saltari et al., 2016). Interestingly, CD271 expression considerably increased from DC to RC melanomas, whereas it decreased from RC to CT and DN melanomas (Figure 1b).

To further define the biological behavior of RCM subtypes, freshly isolated cells from melanoma biopsies were seeded as multicellular tumor spheroids (Figure 1c). Although CT and DN melanoma cells were able to generate spheroids, DC and RC melanoma cells failed to form compact multicellular tumor spheroids, probably owing to their less proliferative capacity (Figure 1d). Consistently, CT and DN melanoma cells showed greater proliferative ability than DC and RC melanoma cells (Figure 1e).

Altogether, these data suggest that CT and DN melanomas contain the most aggressive tumor cell populations. Notably, DN melanoma cells showed the highest expression levels of the melanoma-initiating cell markers CD133 and SOX-2 than the other RCM subtypes, indicating the peculiarity of this melanoma subtype.

RCM subtypes display different gene expression profiles

Given that RCM melanoma subtypes showed differences in terms of tumor aggressiveness, we decided to evaluate the modulation of genes typically involved in the cancer progression process. To this purpose, transcriptome analysis was performed using Nanostring PanCancer Progression Panel, which focuses on 770 genes involved in each phase of cancer progression. Clustering analysis of the gene expression profile for each RCM subtype revealed the existence of four defined transcriptional signatures (Figure 2a). In detail, we found a cluster between DC–RC and CT–DN melanomas, revealing major similarities between these RCM subtypes.

Table 1. Association between RCM Melanoma Subtypes and Clinical Characteristics

	DC (n = 25)		RC (n = 25)		DN (n = 15)		CT (n = 25)		Total (n = 90)		*P*-Value
Age, y, mean ± SD (range)	69.2 ± 12.2 (47–88)		52.6 ± 15.9 (30–89)		55.6 ± 15.3 (31–78)		64 ± 18.2 (24–90)		60.9 ± 16.8 (24–90)		0.001
	N	%	N	%	N	%	N	%	N	%	*P*-Value
Sex											
Female	8	32.0	12	48.0	7	46.7	8	32.0	35	38.9	0.521
Male	17	68.0	13	52.0	8	53.3	17	68.0	55	61.1	
Tumor type											
MIS	11	44.0	0	0	0	0	0	0	11	12.2	
RGP	12	48.0	14	56.0	1	6.7	1	4.0	28	31.1	<0.001
VGP	2	8.0	11	44.0	14	93.3	24	96.0	51	56.7	
Tumor site											
Arts	4	16.0	10	40.0	8	53.3	10	40.0	32	35.6	0.022
Face	7	28.0	0	0.0	1	6.7	2	8.0	10	11.1	
Trunk	14	56.0	15	60.0	6	40.0	13	52.0	48	53.3	
BRAF ^{V600E}	6	24.0	18	72.0	7	58.3	14	56.0	45	51.1	0.007
Breslow index N, mean ± SD (range)	25, 0.2 ± 0.3 (0–1.04)		25, 0.6 ± 0.4 (0–2)		15, 5.8 ± 7.1 (0.65–24)		25, 2.6 ± 2.0 (0.5–8)		90, 2.3 ± 2.5 (0–24)		<0.001
	N	%	N	%	N	%	N	%	N	%	
Breslow index											
mm ≤ 1	24	88.0	22	88.0	1	6.7	5	20.0	50	55.6	<0.001
1 < mm ≤ 2	1	4.0	3	12.0	3	20.0	8	32.0	15	16.7	
2 < mm ≤ 4	0	0.0	0	0.0	6	40.0	7	28.0	13	14.4	
5 < mm ≤ 10	0	0.0	0	0.0	2	13.3	0	0.0	2	2.2	
mm > 10	0	0.0	0	0.0	3	20.0	5	20.0	8	8.9	
Clark level											
I	11	44.0	1	4.0	0	0.0	0	0.0	12	13.3	<0.001
II	11	44.0	12	48.0	1	6.7	1	4.0	25	27.8	
III	3	12.0	10	40.0	5	33.3	8	32.0	26	28.9	
IV	0	0.0	2	8.0	7	46.7	13	52.0	22	24.4	
V	0	0.0	0	0.0	2	13.3	3	12.0	5	5.6	
Mitotic index											
0–1	24	96.0	24	96.0	5	33.3	9	36.0	60	68.9	<0.001
2–5	1	4.0	1	4.0	7	46.7	10	40.0	19	21.1	
>5	0	0.0	0	0.0	3	20.0	6	24.0	9	10.0	
Previous history of melanoma	9	36.0	2	8.0	1	6.7	0	0.0	12	13.3	0.001
Positive sentinel lymph node	0	0.0	2	8.0	4	26.7	8	32.0	14	15.6	0.013
New melanoma	10	40.0	2	8.0	4	26.7	3	12.0	17	21.1	0.024
Metastasis 0–5 y	0	0.0	1	4.0	5	33.3	5	20.0	11	12.2	0.005

Abbreviations: CT, combined type; DC, dendritic cell; DN, dermal nest; MIS, melanoma in situ, N, number of samples; RC, round cell; RCM, reflectance confocal microscopy; RGP, radial growth phase; VGP, vertical growth phase; y, year.

Previous history of melanoma includes tumors diagnosed before that used in the study. New melanoma includes tumors developed after diagnosis of the lesion employed in the study (another anatomical site). Metastasis 0–5 years indicates distal metastases developed in several parts of the body from 0 to 5 years after primary diagnoses.

To determine the biological processes (BPs) associated with each RCM subtype, we performed a Gene Ontology (GO) term enrichment using DAVID functional annotation tool. According to the Nanostring panel, the main gene modulation was found in genes involved in extracellular matrix (ECM) remodeling, angiogenesis, and inflammation GO BP terms (Figure 2b). Moreover, modulation of genes related to cancer-associated transcription factors was identified between the different melanoma groups. Interestingly, we observed a progressive upregulation in ECM remodeling, angiogenesis, and inflammation BP terms from DC to CT melanomas. Conversely, a downregulation of the genes involved in cell adhesion was found from DC to CT melanomas. DN gene expression profile appeared to deviate from the other RCM subtypes, showing a distinct pattern associated with ECM remodeling, angiogenesis, inflammation, and cell adhesion (Figure 2b). In addition, SMAD and BMP signaling pathways, stem cell differentiation, bicellular tight junction assembly, and positive regulation of cell differentiation were the most significantly modulated transcription factor–associated genes. This is consistent with the functional role of those genes in tumor progression (Rusciano, 2000; Tuncer et al., 2019; Venkatesan et al., 2018).

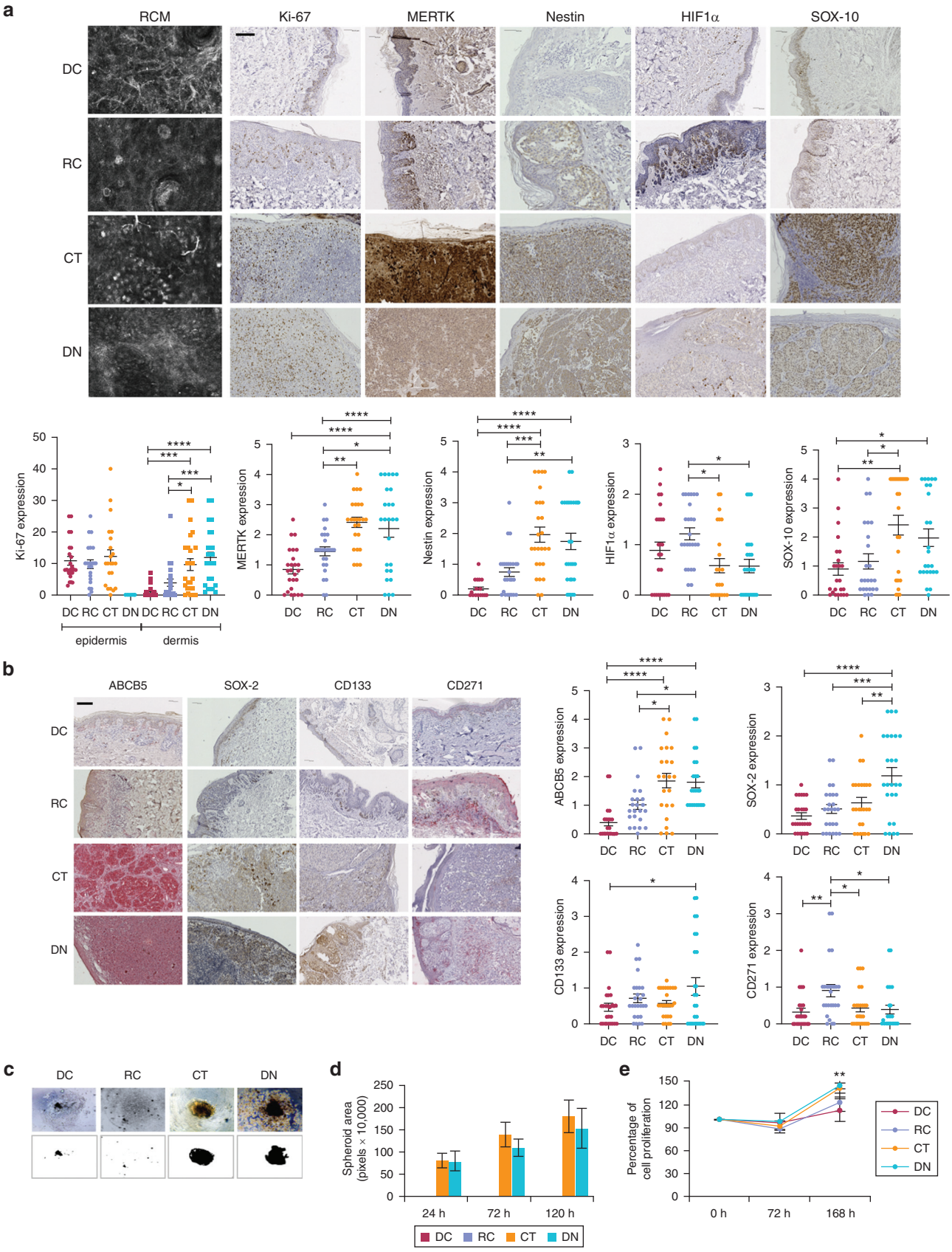

Figure 1. Correlation between RCM melanoma subtypes with markers expression and biological behavior in vitro. (**a, b**) RCM images (Vivascope 1500) and expression of aggressiveness and stemness markers evaluated by IHC. Bar = 50 μm. Data represent the mean ± SEM for each RCM subtype (25 per group, 15 for DN melanoma). Two-way ANOVA was used for statistical analyses. *0.01 ≤ P ≤ 0.05, **0.001 ≤ P ≤ 0.01, and ***P ≤ 0.001. (**c**) Melanoma biopsies were digested, and approximately 10^4 cells were seeded for spheroid formation. (**d**) Total spheroids area was measured by ImageJ software, and (**e**) MTT assay was

Because DC melanoma seems to be the less aggressive melanoma subtype, we evaluated the gene expression profile of each melanoma group compared with that of the DC type (Figure 2c and d). By uploading the most significantly upregulated and downregulated genes for each melanoma subtype compared with those of DC melanoma into Venny 2.1, we identified 55 (25.6%) and 60 (27.97%) genes that were specifically upregulated in RC and CT melanomas, respectively, versus in DC melanoma. On the contrary, only 16 genes (7.4%) were upregulated in DN melanoma versus in DC melanoma. Conversely, 128 genes (68.5%) were downregulated in DN melanoma versus in DC melanoma, whereas only 7 (2.7%) and 18 (6.8%) genes were downregulated in RC and CT melanomas, respectively, versus those in DC melanoma.

To highlight the differences between the RCM subtypes, paired comparisons were performed (RC vs. DC, CT vs. DC, DN vs. DC, RC vs. CT, and CT vs. DN), and the top significantly modulated genes for each comparison, as underlined by Volcano plots, underwent GO BP term enrichment (Figure 2d). As expected, slight differences in gene modulation were found in RC melanoma versus in DC melanoma. In this comparison, we found a modulation of genes associated with leukocyte migration, ECM organization, cell–substrate adhesion, and positive regulation of endothelial cell migration GO BP terms, which are key processes during the early phases of tumor progression (Cho et al., 2019; Swierczak et al., 2015; Valastyan and Weinberg, 2011). Conversely, a higher number of genes were significantly modulated in CT than in DC melanoma (Figure 2d), including the genes associated with angiogenesis, ECM organization, cell adhesion, leukocyte migration GO BP terms. These differences were exacerbated in the comparison between DC and DN melanomas (Figure 2d). Finally, clustering analysis representing the main representative GO BP terms for each comparison confirmed the existence of defined transcriptional signatures for each melanoma subtype (Supplementary Figure S2). CT versus DC melanomas and DN versus DC melanomas comparisons showed the most striking differences in the modulation of genes associated with ECM organization, angiogenesis, cell adhesion, and leukocyte migration.

Survivin is considered a biomarker of poor prognosis in melanoma (Takeuchi et al., 2005), and the expression of CXCL8 positively correlates with tumor progression (Ugurel et al., 2001), whereas CD271 downregulation has been associated with melanoma progression and invasion (Saltari et al., 2016). The expression of *BIRC5* (survivin) and *CXCL8* mRNA significantly increased from DC to CT and DN melanomas, suggesting a progressive increase in tumor aggressiveness. On the contrary, *NGFR* mRNA (CD271) increased from DC to RC melanomas and subsequently decreased from RC to CT and DN melanomas in a statistically significant manner, confirming the immunohistochemical results (Figure 2e).

RCM morphology reflects tumor aggressiveness and progression stage

The results mentioned earlier indicate that RC subtype shows intermediate characteristics between DC and CT melanomas. To validate this finding, a volcano plot was generated with the most modulated genes in RC versus CT melanomas comparison, and GO BP terms enrichment was performed for the most relevant genes (Figure 3a). Genes associated with angiogenesis and cell proliferation pathway (i.e., *MAPKs*) were the most significantly modulated. During tumor progression, highly proliferating neoplastic cells must acquire the capacity to induce angiogenesis to meet their growing demands for nutrients and oxygen and continue proliferation. Moreover, angiogenesis is an important indicator of tumor aggressiveness and poor clinical outcome in various solid tumors (Cho et al., 2019).

Recently, we have shown that CD271 downregulation plays a role in promoting melanoma progression and invasion, at least in part because of the lack of cell–cell adhesion molecules (Saltari et al., 2016). However, CD271 expression increased from DC to RC melanomas and subsequently turned off from RC to CT melanoma (Figures 1b and 2d). Moreover, we observed that CD271 expression increased with BI in DC and RC subtypes, whereas its expression inversely correlated with BI in CT tumors (BI $>$ 1 mm) (Figure 3b and c). At the same time, we found that E-cadherin expression significantly decreased from DC to CT melanomas, suggesting a progressive loss of epithelial cell adhesion molecules, which was paralleled by an increase of N-cadherin from CT to DC melanomas (Figure 3d). Altogether, these data suggest the progressive increase of aggressiveness from DC to RC and CT subtypes.

CT and DN subtypes show a different gene expression profile and biological behavior in vitro

Data reported in this study suggest that CT and DN melanomas are the most aggressive tumors, with DN melanoma revealing a unique gene expression profile. To evaluate the difference between these tumor types, a volcano plot was generated with the most modulated genes in CT versus DN melanomas comparison, and GO BP terms enrichment was performed for the most relevant genes. The gene associated with angiogenesis, ECM organization, disassembly of cell adhesion, and inflammation were the most significantly modulated (Figure 4a).

To further investigate the difference between these tumors, we evaluated their invasive capacity in vitro using three-dimensional models (Supplementary Figure S3a and Figure 4b). We found that DN melanoma was significantly more invasive than CT melanoma (Figure 4c–e). Moreover, DN melanoma cells reached a longer distance from the spheroids than CT melanoma cells (Figure 4f). In melanoma skin reconstructs, CT melanoma cells were observed at the dermal–epidermal junction. On the contrary, DN cells were able to grow only when seeded directly into the dermis (Figure 4g). Both tumors display high proliferative capacity in

performed at different time points. Data represent the mean ± SD of three independent biological experiments of at least three different biopsies per group. Student's *t*-test was used for statistical analyses. *$0.01 \leq P \leq 0.05$ and **$0.001 \leq P \leq 0.01$. CT, combined-type; DC, dendritic cell; DN, dermal nest; h, hour; IHC, immunohistochemistry; RC, round cell; RCM, reflectance confocal microscopy.

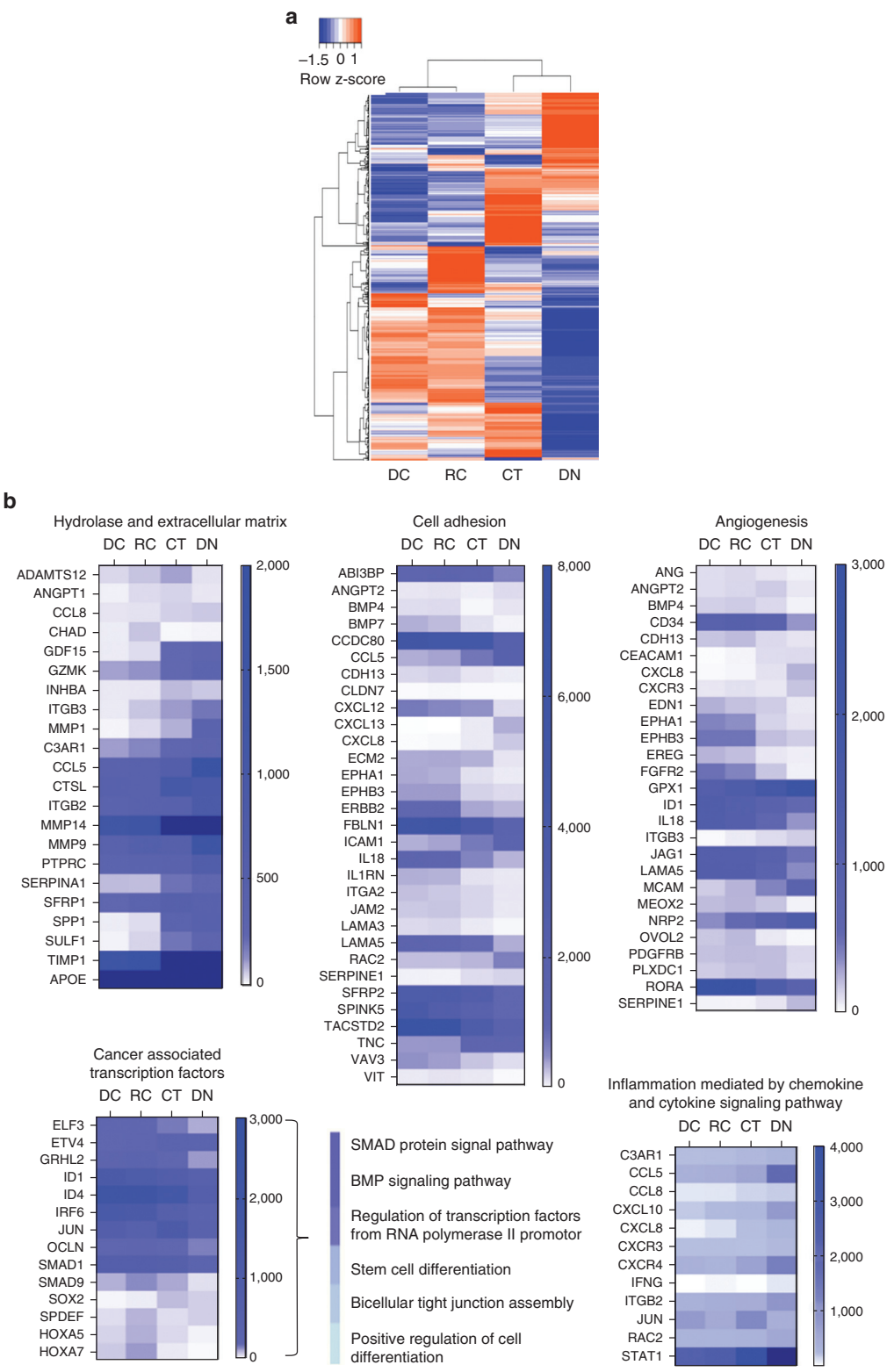

Figure 2. Gene expression profile of RCM melanoma subtypes. (**a**) Clustering analysis of RCM melanoma subtypes. (**b**) Heatmaps representing the main GO BP terms. Gene expression values for each heatmap were ranked according to their z-score after normalization. The gene expression was shown as the raw value of normalized intensity. (**c**) Venny diagram representing the upregulated and downregulated genes in each melanoma subtype compared with those in DC melanoma. (**d**) Volcano plot and GO BP term enrichment of the most significant modulated genes ($-\log_{10} P > 1.27$) in RC versus DC, CT versus DC, and DN versus DC melanomas comparison. (**e**) *BIRC5* (survivin), *CXCL8*, and *NGFR* (CD271) mRNA expression evaluated by real-time PCR in each RCM melanoma subtype. β-actin was used as a reference gene. Data represent the mean ± SD of three independent experiments of three different biopsies per group. Student's *t*-test was used for statistical analyses. *$0.01 \leq P \leq 0.05$ and **$0.001 \leq P \leq 0.01$. BP, biological process; CT, combined-type; DC, dendritic cell; DN, dermal nest; GO, Gene Ontology; RC, round cell; RCM, reflectance confocal microscopy; RQ, relative protein quantity.

skin reconstructs (Supplementary Figure S3b and Figure 4h). E-cadherin was scarcely detected in DN melanoma, which expressed elevated levels of N-cadherin, compared with that in CT melanoma. The higher expression of α_4 and α_7 integrins in DN than in CT melanoma confirmed the greater invasive behavior of this tumor (Haass et al., 2005) (Supplementary Figure S3b and Figure 4h). In addition, DN melanoma expressed significantly increased levels of SOX-2 compared with CT melanoma, confirming its more undifferentiated state (Supplementary Figure S3b and Figure 4h). Finally, invading cells from DN melanoma spheroids expressed a higher level of α_4 integrin, confirming the aggressiveness of this tumor type, and CD271 was scarcely detectable in these cells (Figure 4i).

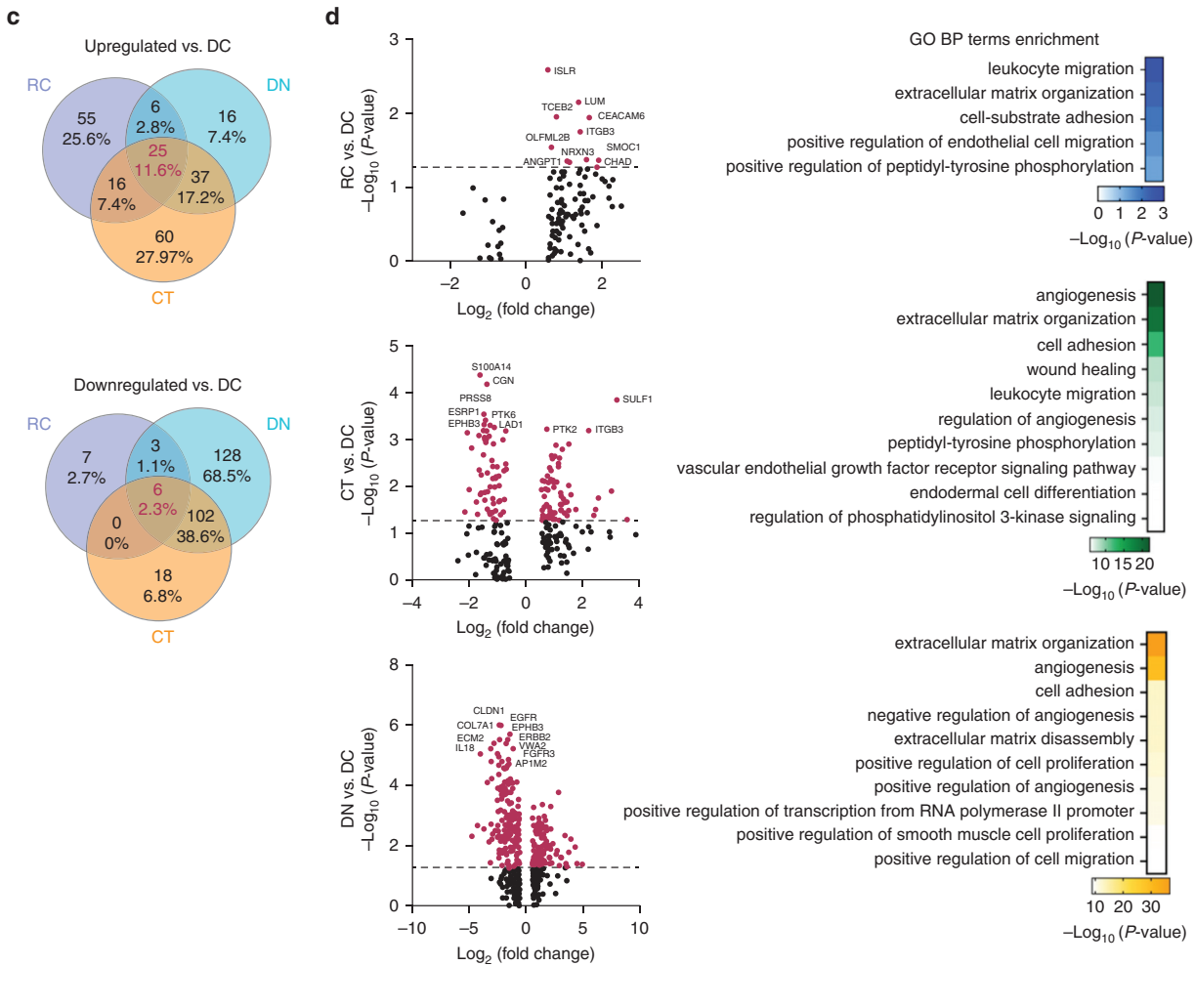

Figure 2. Continued.

DISCUSSION

Melanoma progression depends on diverse phases where the stepwise acquisition of genetic abnormalities contributes to the increase of aggressiveness (Eddy et al., 2021). Distinguishing between these stages may be relevant for a more accurate diagnosis and prognosis.

RCM allows for the identification of four distinct melanoma subtypes, which reflects specific clinical patterns (Pellacani et al., 2014). However, the existence of a close correlation among RCM subtypes, genetic signature, and biological behavior has not been clarified yet.

In this study, we found significant differences in terms of tumor markers expression, modulation of cancer progression–associated genes, and biological behavior in vitro among the RCM melanoma subtypes. In substance, we were able to define a specific biomolecular profile for each melanoma subtype (Figure 5).

Radial growth phase is the first step of melanoma progression, being characterized by the proliferation of atypical melanocytes in the epidermis. This is followed by the vertical growth phase, which consists of proliferating tumor cells in the dermis (Clark et al., 1969). In this context, Ki-67–positive cells define tumor proliferation compartments in melanomas (Gimotty et al., 2005). The presence of proliferating cells in the dermis in CT and DN melanomas suggests the higher aggressiveness of these tumors than that of DC and RC subtypes. In addition, the expression of a small fraction of Ki-67–positive cells in the dermis in RC versus DC melanomas suggests that RC melanoma is more advanced than DC type. Indeed, DC melanoma is mainly a slow

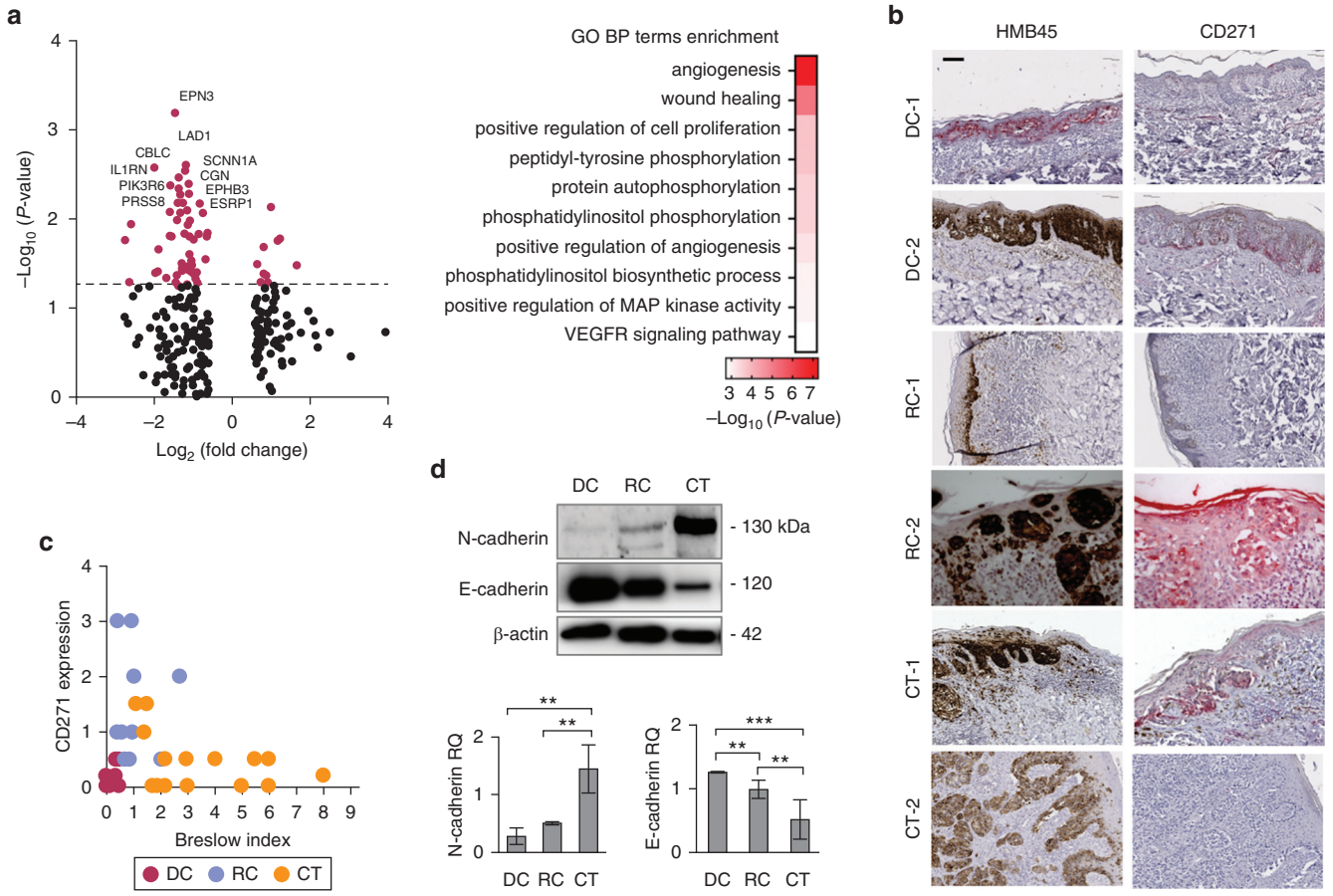

Figure 3. Correlation between RCM-observed morphology and tumor aggressiveness. (**a**) Volcano plot and GO BP term enrichment of the most significantly modulated genes ($-\log_{10} P > 1.27$) in RC versus CT melanomas comparison. (**b**) Representative image of HMB45 and CD271 expression on DC, RC, and CT melanoma subtypes. Bar = 50 μm. (**c**) Correlation between Breslow index and CD271 expression level. (**d**) Representative image and RQ of immunoblotting showing the expression of E- and N-cadherin. Proteins were extracted from at least three different DC, RC, and CT melanomas cryopreserved biopsies. β-actin was used as a normalizing protein. BP, biological process; CT, combined-type; DC, dendritic cell; GO, Gene Ontology; RC, round cell; RCM, reflectance confocal microscopy; RQ, relative protein quantity.

intraepidermal growing tumor characterized by single-cell proliferation, whereas RC melanoma shows a predominantly horizontal pattern of growth with a tendency to form nests and to infiltrate the dermis (Pellacani et al., 2014). Moreover, patients with DC melanoma developed more melanomas, mainly melanoma in situ, than those with the other RCM subtypes, suggesting an association with prolonged sun exposure. In fact, DC melanoma is most frequent in elderly patients with a history of more intense solar exposure (Grazziotin et al., 2016).

Conversely, CT and DN melanomas, characterized by a high level of Ki-67–positive cells in the dermis, metastasized at a significantly higher rate than DC or RC melanomas, suggesting a more aggressive behavior. The expression of MERTK and Nestin as well as the high levels of *CXCL8* and *BIRC5* mRNA underline the increase of aggressive features from DC to CT melanomas, which is also confirmed by their proliferative capacity in vitro. In addition, CT and DN melanomas are characterized by more elevated levels of ABCB5, a marker of highly aggressive melanomas characterized by chemoresistance (Schatton et al., 2008). CD271 downregulation has been shown to promote melanoma progression and invasion at least in part owing to the lack of cell–cell adhesion (Saltari et al., 2016). However, CD271 expression considerably increased from DC to RC melanomas, whereas it decreased from RC to CT and DN melanomas. Therefore, we hypothesized that CD271 could have a switch on–off function during melanoma progression. In fact, the increased CD271 expression in RC melanoma could be instrumental in favoring its epidermis-to-dermis transition, involving changes in cell–cell adhesion molecules. During melanoma progression, modulation of cell adhesion molecules is known to guide the phenotypic change that promotes cell migration (Caramel et al., 2013). The switching from E-cadherin to N-cadherin from DC to CT melanomas confirms the existence of a shift in cell–cell adhesion molecules between these tumor types. In addition, the higher expression of HIF1α in RC melanoma could be necessary for the acquisition of the invasive properties and the need for new vascularization (Widmer et al., 2013) On the contrary, CD271 expression decreases in DN and CT types, favoring a more aggressive and invasive phenotype, in line with the results of our previous work (Saltari et al., 2016).

Altogether, our results strongly suggest the existence of a close correlation between RCM-observed cell morphology and tumor aggressiveness. Given its slow-growing features,

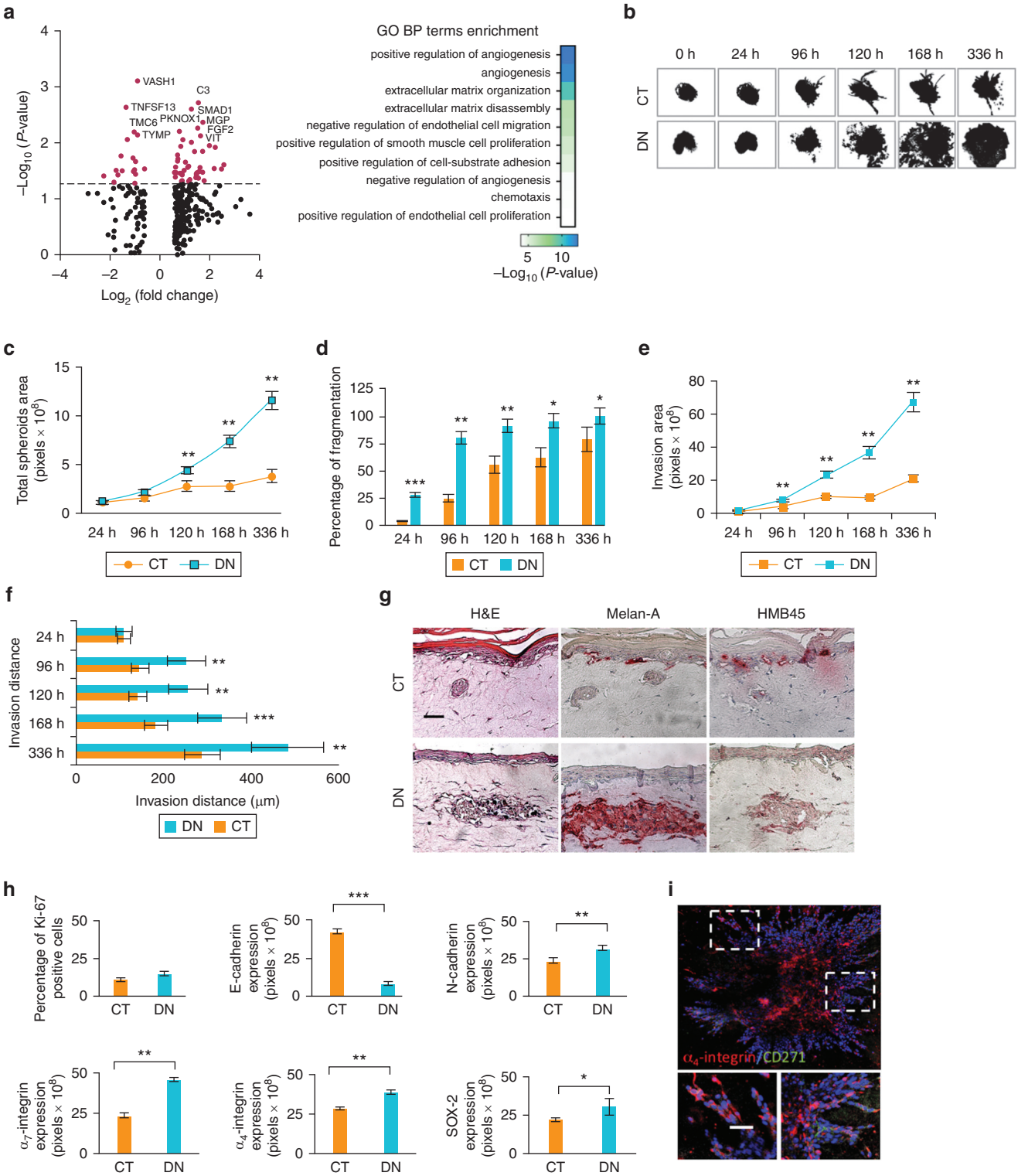

Figure 4. Differences between the most aggressive RCM melanoma subtypes. (**a**) Volcano plot and GO BP term in CT versus DN melanomas comparison. (**b**) CT and DN melanomas spheroids invasion assay. (**c**) Graphical representation of total spheroids area, (**d**) percentage of fragmentation, (**e**) cells invading the area, and (**f**) invasion distance. (**g**) H&E, melan-A, and HMB-45 staining of CT and DN melanoma skin reconstruct. Bar = 50 μm. (**h**) Expression of MIB/Ki-67, E-/N-cadherin, α_7 integrin, α_4 integrin, and SOX-2 in CT and DN melanoma skin reconstruct. (**i**) Expression of α_4 integrin (red) and CD271 (green) in DN melanoma spheroids implanted in type I collagen matrix. Bar = 100 μm. Data represent the mean ± SD of a triplicate determination of at least three biopsies per group. Student's *t*-test was used for statistical analyses. *$0.01 \leq P \leq 0.05$, **$0.001 \leq P \leq 0.01$, and ***$P \leq 0.001$. BP, biological process; CT, combined-type; DN, dermal nest; GO, Gene Ontology; h, hour; RCM, reflectance confocal microscopy.

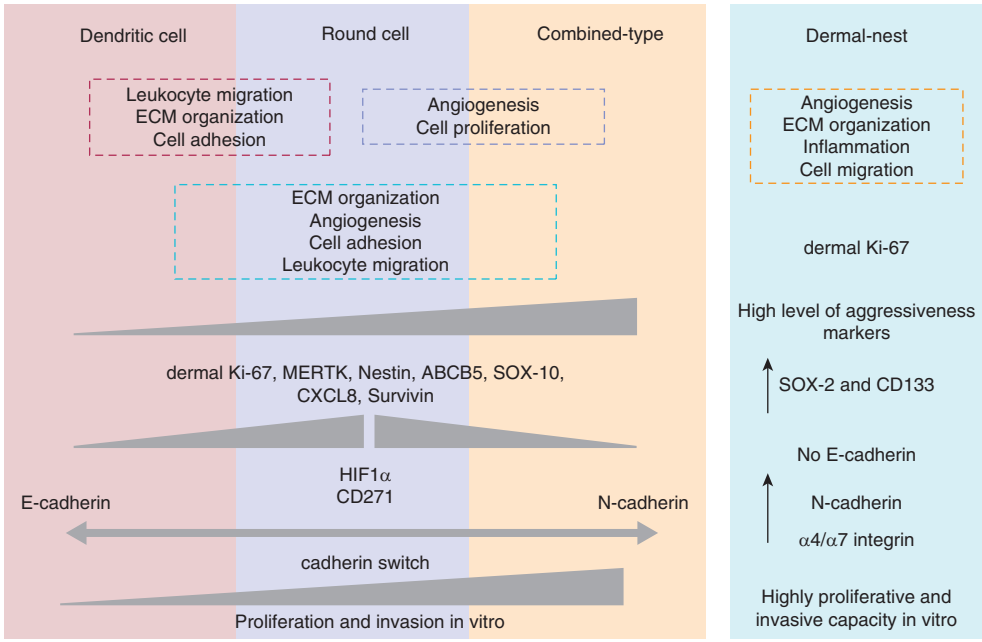

Figure 5. Schematic representation of the biomolecular features identified for each RCM melanoma subtype. SOX-2 and CD133 are stemness markers; MERTK, nestin, dermal Ki-67, SOX-10, CXCL8, and survivin are aggressiveness markers. CD271 is a progression and invasion marker. HIF1α is a hypoxia and angiogenesis marker. E-cadherin to N-cadherin switch and α_4/α_7 integrin are EMT process/progression and invasion markers. ECM, extracellular matrix; EMT, epithelial to mesenchymal transition; RCM, reflectance confocal microscopy.

DC melanoma may represent the less aggressive and well-differentiated type of melanoma, with limited abilities of proliferation and invasion (Argenziano et al., 2010). Conversely, a tumor that arises with a predominant RC population has a faster pattern of growth and a shorter time to invasion and may present an intermediate degree of aggressiveness between DC-type and the most invasive CT and DN melanomas. Melanoma cells in DC or RC types may undergo a dedifferentiation step, creating less cohesive cells aggregated into the dermis, corresponding to CT melanoma (Longo et al., 2013). This hypothesis could be confirmed by the higher expression of stemness markers in CT than in DC and RC melanomas.

This study also shows that DN melanoma is a unique tumor subtype with peculiar features. Although CT melanomas may share some morphological characteristics with the DN subtype, that is, small cell dermal aggregates called cerebriform nests (Pellacani et al., 2005), biomolecular markers are significantly different. In fact, DN melanomas present Ki-67–positive cells only in the dermis and express the highest levels of the melanoma-initiating cells markers, indicating a more undifferentiated state. Moreover, DN melanomas are significantly more invasive than CT melanomas in vitro, as confirmed by the higher expression of α_4/α_7 integrin. Interestingly, DN melanoma cells are able to attach and grow only when seeded directly into the dermis in skin reconstructs. Accordingly, E-cadherin, an epithelial adhesion molecule (van Roy, 2014), was scarcely detected in DN melanoma. The peculiar features of DN melanoma are coherent with the idea of the different origins of this tumor. It could probably originate directly from dermal stem cells without an epidermal radial growth phase (Hoerter et al., 2012; Zalaudek et al., 2008).

In conclusion, we believe that there are at least two main melanoma subtypes: (i) the one originating in the epidermis, which may arise as DC or RC type, with the potential to progress into the CT type, developing invasive clones morphologically similar to those of DN-type melanoma but with different biomolecular profiles, and (ii) the type initiating in the dermis, characterized by DN melanoma morphology on RCM and the most aggressive biomolecular profile.

This work represents the most comprehensive study on the correlation between RCM-observed cell morphology and biomolecular behavior of melanoma, which accounts for a diverse degree of tumor aggressiveness. Moreover, these data confirm that RCM can be a dependable tool for detecting different types of melanomas and for screening purposes. The findings of this study represent a first step to the creation of an integrated clinical/biomolecular model of melanoma classification for reaching a more accurate patient-/tumor-tailored therapeutic approach.

MATERIALS AND METHODS

Melanoma cases selection

A total of 90 patients with melanoma were randomly selected at the Department of Dermatology of the University of Modena and Reggio Emilia (Modena, Italy) and Sassuolo Hospital (Modena, Italy). Melanoma biopsies were collected after patients provided informed written consent approved by the Ethical Committee of Area Vasta Emilia Nord (protocol number 475, Doc. 118/14 — 09/02/2016). Immunohistochemistry, culture methods, and in vitro assay are fully described in Supplementary Materials and Methods.

Real-time PCR, nanostring, and computational analysis

A total of 32 samples were employed (9 for DC, 6 for RC, 7 for DN, and 10 for CT melanomas). Total RNA was extracted from formalin-fixed, paraffin-embedded melanoma samples as reported in Supplementary Materials and Methods. Real-time PCR was performed as previously reported (Quadri et al., 2021). Primers sequences are listed in Supplementary Table S1.

Transcriptomic analysis of RCM subtypes was performed at PharmaDiagen (Pordenone, Italy) using the nCounter Nanostring technology platform. Gene expression clustering analysis was performed on the normalized gene means by Heatmapper (Babicki

et al., 2016). The most significantly modulated genes were determined by fold change of ±1.5 and $P < 0.05$ (cut-off count > 30). GO BP terms enrichment was obtained by DAVID functional annotation tools (https://david.ncifcrf.gov). Differentially upregulated and downregulated genes were evaluated by Venny 2.1 (http://bioinfogo.cnb.csic.es/tools/venny). Volcano plots were generated by Prism 9 (GraphPad Software, La Jolla, CA). Details are provided in Supplementary Materials and Methods.

Western blotting

Total proteins were extracted from at least three cryopreserved melanoma biopsies per subtype. Protein quantification and western blot were performed as previously indicated (Quadri et al., 2021). The primary antibodies are listed in Supplementary Table S2.

Statistical analysis

Statistical analysis was performed using STATA software 14 (StataCorp, College Station, TX) or Prism 9 (GraphPad Software) as indicated in Supplementary Materials and Methods. Data were considered significant with $*0.01 \leq P \leq 0.05$, $**0.001 \leq P \leq 0.01$, and $***P \leq 0.001$.

Data availability statement

Data supporting the findings of this study are available from the corresponding author on reasonable request. Datasets related to this study can be found at (https://www.ncbi.nlm.nih.gov/geo/query/acc.cgi?acc=GSE174395).

ORCIDs

Alessandra Marconi: http://orcid.org/0000-0002-5667-5766
Marika Quadri: http://orcid.org/0000-0001-7619-660X
Francesca Farnetani: http://orcid.org/0000-0001-7088-9077
Silvana Ciardo: http://orcid.org/0000-0002-2381-2189
Elisabetta Palazzo: http://orcid.org/0000-0002-0812-5524
Roberta Lotti: http://orcid.org/0000-0003-2126-4147
Anna Maria Cesinaro: http://orcid.org/0000-0001-6807-8152
Luca Fabbiani: http://orcid.org/0000-0002-0104-5249
Cristina Vaschieri: http://orcid.org/0000-0001-6434-2681
Mario Puviani: http://orcid.org/0000-0003-1792-2581
Cristina Magnoni: http://orcid.org/0000-0002-6081-4925
Shaniko Kaleci: http://orcid.org/0000-0002-1166-2961
Carlo Pincelli: http://orcid.org/0000-0003-4416-2637
Giovanni Pellacani: http://orcid.org/0000-0002-7222-2951

CONFLICT OF INTEREST

The authors state no conflict of interest.

ACKNOWLEDGMENTS

This work was supported by the AIRC (Associazione Italiana per la Ricerca sul Cancro) Investigator Grant - IG 2015 (number 16890).

AUTHOR CONTRIBUTIONS

Conceptualization: AM, FF, CP, GP; Data Curation: MQ, AM; Formal Analysis: MQ, AM, EP, SC, FF, GP; Funding Acquisition: GP; Investigation: MQ, AM, EP, FF, CP, GP; Methodology: MQ, AM, EP, SC, FF, RL, MP, CM, AMC, LF, CV, SK; Resources: AM, CP, GP; Writing - Original Draft Preparation: MQ; Writing - Review and Editing: MQ, AM, FF, SC, EP, RL, AMC, LF, CV, SK, CP, GP

SUPPLEMENTARY MATERIAL

Supplementary material is linked to the online version of the paper at www.jidonline.org, and at https://doi.org/10.1016/j.jid.2021.12.024.

REFERENCES

Argenziano G, Kittler H, Ferrara G, Rubegni P, Malvehy J, Puig S, et al. Slow-growing melanoma: a dermoscopy follow-up study. Br J Dermatol 2010;162:267–73.

Babicki S, Arndt D, Marcu A, Liang Y, Grant JR, Maciejewski A, et al. Heatmapper: web-enabled heat mapping for all. Nucleic Acids Res 2016;44:W147–53.

Beretti F, Bertoni L, Farnetani F, Pellegrini C, Gorelli G, Cesinaro AM, et al. Melanoma types by in vivo reflectance confocal microscopy correlated with protein and molecular genetic alterations: a pilot study. Exp Dermatol 2019;28:254–60.

Boiko AD, Razorenova OV, van de Rijn M, Swetter SM, Johnson DL, Ly DP, et al. Human melanoma-initiating cells express neural crest nerve growth factor receptor CD271 [published correction appear in Nature 2011;470:424]. Nature 2010;466:133–7.

Caramel J, Papadogeorgakis E, Hill L, Browne GJ, Richard G, Wierinckx A, et al. A switch in the expression of embryonic EMT-inducers drives the development of malignant melanoma. Cancer Cell 2013;24:466–80.

Cho WC, Jour G, Aung PP. Role of angiogenesis in melanoma progression: update on key angiogenic mechanisms and other associated components. Semin Cancer Biol 2019;59:175–86.

Clark WH Jr, From L, Bernardino EA, Mihm MC. The histogenesis and biologic behavior of primary human malignant melanomas of the skin. Cancer Res 1969;29:705–27.

Eddy K, Shah R, Chen S. Decoding melanoma development and progression: identification of therapeutic vulnerabilities. Front Oncol 2021;10:626129.

Fink C, Haenssle HA. Non-invasive tools for the diagnosis of cutaneous melanoma. Skin Res Technol 2017;23:261–71.

Gershenwald JE, Scolyer RA, Hess KR, Sondak VK, Long GV, Ross MI, et al. Melanoma staging: evidence-based changes in the American Joint Committee on Cancer eighth edition cancer staging manual. CA Cancer J Clin 2017;67:472–92.

Gimotty PA, Van Belle P, Elder DE, Murry T, Montone KT, Xu X, et al. Biologic and prognostic significance of dermal Ki67 expression, mitoses, and tumorigenicity in thin invasive cutaneous melanoma. J Clin Oncol 2005;23:8048–56.

Graf SA, Busch C, Bosserhoff AK, Besch R, Berking C. SOX10 promotes melanoma cell invasion by regulating melanoma inhibitory activity. J Invest Dermatol 2014;134:2212–20.

Grazziotin TC, Alarcon I, Bonamigo RR, Carrera C, Potrony M, Aguilera P, et al. Association between confocal morphologic classification and clinical phenotypes of multiple primary and familial melanomas. JAMA Dermatol 2016;152:1099–105.

Haass NK, Smalley KS, Li L, Herlyn M. Adhesion, migration and communication in melanocytes and melanoma. Pigment Cell Res 2005;18:150–9.

Hoerter JD, Bradley P, Casillas A, Chambers D, Denholm C, Johnson K, et al. Extrafollicular dermal melanocyte stem cells and melanoma. Stem Cells Int 2012;2012:407079.

Inumaru JS, Gordo KI, Fraga Junior AC, Silva AMTC, Leal CBQS, Ayres FM, et al. Analysis of the BRAF V600E mutation in primary cutaneous melanoma. Genet Mol Res 2014;13:2840–8.

Jenkins RW, Fisher DE. Treatment of advanced melanoma in 2020 and beyond. J Invest Dermatol 2021;141:23–31.

Longo C, Farnetani F, Ciardo S, Cesinaro AM, Moscarella E, Ponti G, et al. Is confocal microscopy a valuable tool in diagnosing nodular lesions? A study of 140 cases. Br J Dermatol 2013;169:58–67.

Monzani E, Facchetti F, Galmozzi E, Corsini E, Benetti A, Cavazzin C, et al. Melanoma contains CD133 and ABCG2 positive cells with enhanced tumourigenic potential. Eur J Cancer 2007;43:935–46.

Pellacani G, Cesinaro AM, Seidenari S. In vivo assessment of melanocytic nests in nevi and melanomas by reflectance confocal microscopy. Mod Pathol 2005;18:469–74.

Pellacani G, De Pace B, Reggiani C, Cesinaro AM, Argenziano G, Zalaudek I, et al. Distinct melanoma types based on reflectance confocal microscopy. Exp Dermatol 2014;23:414–8.

Quadri M, Lotti R, Bonzano L, Ciardo S, Guanti MB, Pellacani G, et al. A novel multi-action emollient plus cream improves skin barrier function in patients with atopic dermatitis: in vitro and clinical evidence. Skin Pharmacol Physiol 2021;34:8–18.

Rusciano D. Differentiation and metastasis in melanoma. Crit Rev Oncog 2000;11:147–63.

Saltari A, Truzzi F, Quadri M, Lotti R, Palazzo E, Grisendi G, et al. CD271 down-regulation promotes melanoma progression and invasion in three-dimensional models and in zebrafish. J Invest Dermatol 2016;136:2049–58.

Santini R, Pietrobono S, Pandolfi S, Montagnani V, D'Amico M, Penachioni JY, et al. SOX2 regulates self-renewal and tumorigenicity of human melanoma-initiating cells. Oncogene 2014;33:4697–708.

Schatton T, Murphy GF, Frank NY, Yamaura K, Waaga-Gasser AM, Gasser M, et al. Identification of cells initiating human melanomas. Nature 2008;451:345–9.

Schlegel J, Sambade MJ, Sather S, Moschos SJ, Tan AC, Winges A, et al. MERTK receptor tyrosine kinase is a therapeutic target in melanoma. J Clin Invest 2013;123:2257–67.

Scolyer RA, Long GV, Thompson JF. Evolving concepts in melanoma classification and their relevance to multidisciplinary melanoma patient care. Mol Oncol 2011;5:124–36.

Swierczak A, Mouchemore KA, Hamilton JA, Anderson RL. Neutrophils: important contributors to tumor progression and metastasis. Cancer Metastasis Rev 2015;34:735–51.

Takeuchi H, Morton DL, Elashoff D, Hoon DS. Survivin expression by metastatic melanoma predicts poor disease outcome in patients receiving adjuvant polyvalent vaccine. Int J Cancer 2005;117:1032–8.

Tuncer E, Calçada RR, Zingg D, Varum S, Cheng P, Freiberger SN, et al. SMAD signaling promotes melanoma metastasis independently of phenotype switching. J Clin Invest 2019;129:2702–16.

Ugurel S, Rappl G, Tilgen W, Reinhold U. Increased serum concentration of angiogenic factors in malignant melanoma patients correlates with tumor progression and survival. J Clin Oncol 2001;19:577–83.

Valastyan S, Weinberg RA. Tumor metastasis: molecular insights and evolving paradigms. Cell 2011;147:275–92.

van Roy F. Beyond E-cadherin: roles of other cadherin superfamily members in cancer. Nat Rev Cancer 2014;14:121–34.

Venkatesan AM, Vyas R, Gramann AK, Dresser K, Gujja S, Bhatnagar S, et al. Ligand-activated BMP signaling inhibits cell differentiation and death to promote melanoma. J Clin Invest 2018;128:294–308.

Viros A, Fridlyand J, Bauer J, Lasithiotakis K, Garbe C, Pinkel D, et al. Improving melanoma classification by integrating genetic and morphologic features. PLoS Med 2008;5:e120.

Whiteman DC, Pavan WJ, Bastian BC. The melanomas: a synthesis of epidemiological, clinical, histopathological, genetic, and biological aspects, supporting distinct subtypes, causal pathways, and cells of origin. Pigment Cell Melanoma Res 2011;24:879–97.

Widmer DS, Hoek KS, Cheng PF, Eichhoff OM, Biedermann T, Raaijmakers MIG, et al. Hypoxia contributes to melanoma heterogeneity by triggering HIF1α-dependent phenotype switching. J Invest Dermatol 2013;133:2436–43.

Wilson MA, Schuchter LM. Chemotherapy for melanoma. Cancer Treat Res 2016;167:209–29.

Zalaudek I, Marghoob AA, Scope A, Leinweber B, Ferrara G, Hofmann-Wellenhof R, et al. Three roots of melanoma. Arch Dermatol 2008;144:1375–9.

SUPPLEMENTARY MATERIALS AND METHODS

Melanoma cases selection

A total of 90 patients with melanoma were randomly selected at the Department of Dermatology of the University of Modena and Reggio Emilia (Modena, Italy). Clinical, dermoscopic, and reflectance confocal microscopy (RCM) images were acquired through a Canfield Nikon D90 Digital SLR, a Canfield Close-up Scale (Canfield Imaging Systems, Fairfield, NJ), and an RCM laser scanning microscope (Vivascope 1500; MAVIG, Munich, Germany), respectively, and were stored in a dedicated database. RCM employs an 830 nm laser beam with a maximum power of 20 mW. Instrument and acquisition procedures were previously described (Pellacani et al., 2007; Rajadhyaksha et al., 1995). A minimum of three mosaics were obtained per lesion at three different depths, corresponding to the superficial epidermal layer (the stratum granulosum/spinosum), dermal–epidermal junction, and papillary dermis. Each image was blindly evaluated by an expert dermatologist for epidermal, dermal–epidermal junction, and upper dermis architecture and was classified into four melanoma subtypes, as previously reported (Pellacani et al., 2014).

The selected melanoma cases were employed to perform immunohistochemical analysis. Moreover, samples were selected for Nanostring analysis and in vitro experiments on the basis of the sample's availability and quality.

Melanoma biopsies and images were collected after patients provided informed written consent approved by the Ethical Committee of Area Vasta Emilia Nord (protocol number 475, Doc. 118/2014 − 09/02/2016).

Immunohistochemistry

Melanoma markers were detected using UltraView Universal DAB and RED Detection Kit (Ventana Medical Systems, Roche Diagnostics International, Rotkreuz, Switzerland).

The Opti-View DAB immunohistochemistry automated detection kit (Ventana Medical Systems) was employed to evaluate $BRAF^{V600E}$ mutation. Moreover, for some patients (based on clinician decision), $BRAF^{V600E}$ mutation was evaluated at the biomolecular level as routine practices at the Department of Pathology of the University Hospital (Modena, Italy) using the MassARRAY (Sequenom, San Diego, CA).

As concern for CD271, the Fast Red kit UltraVision LP Detection System AP Polymer & Fast Red Chromogen (Thermo Fisher Scientific, Waltham, MA) was used to detect CD271, according to the manufacturer's instructions. The primary antibodies are listed in Supplementary Table S2.

Images of the H&E and immunohistochemistry staining were obtained by a D-Sight slide scanner (Menarini Diagnostics, Firenze, Italy). Protein expression was scored from 0 to 4, and the average positive cells were calculated for each individual melanoma as follow: a score of 0, 0% staining melanoma cells; a score of 1, 1–25% staining positive melanoma cells; a score of 2, 26–50% staining positive melanoma cells; a score of 3, 51–75% staining positive melanoma cells; and a score of 4, 76−100% staining positive melanoma cells.

Melanoma biopsies digestion, culture methods, and in vitro assay

Melanoma biopsies were provided by the Dermatology Surgery of the Policlinic of Modena and Sassuolo Hospital. The use of melanoma biopsies was approved by the Ethical Committee of Area Vasta Emilia Nord (protocol number 475, Doc. 118/2014 − 09/02/2016). A total of 20 samples were employed for in vitro analysis (four for dendritic cell [DC], four for round cell [RC], nine for combined-type [CT], and three for dermal nest [DN] melanomas) on the basis of samples' availability and quality that allowed us to carry out the specific methods adequately.

Biopsies were digested in a mixture of collagenase I and IV (1:2,000 and 1:500, respectively) (Gibco, Thermo Fisher Scientific), and cells were seeded and cultured using hanging drop or liquid overlay methods in RPMI medium supplemented with 10% of heat-inactivated serum, 2% of L-glutamine, and 1% of penicillin/streptomycin (Lonza, Basel, Switzerland). MTT assay was performed to evaluate RCM melanoma spheroids from 24 to 168 hours. Collagen invasion assay was used to assess the invasion ability of melanoma cells within the collagen I matrix. The area occupied by melanoma spheroids and the invasive capacity of cells were evaluated by ImageJ program (National Institutes of Health, Bethesda, MD), as previously indicated (Saltari et al., 2016). Distance reached by cells migrated from spheroids were calculated as previously indicated (Quadri et al., 2022). Briefly, at least three pictures of spheroids for time points were analyzed with GNU Image Manipulation Program (GIMP, Los Angeles, CA). Distance, in millimeters, was measured from the edge of the spheroid in the four directions using the tool Measure. The invasion distances at different time points were normalized on time 0. Three different biological replicates were performed.

NanoString and computational analyses

Total RNA was extracted from formalin-fixed, paraffin-embedded samples using RNeasy FFPE kit (Qiagen, Hilden, Germany), following the manufacturer's instruction. A total of 32 samples were employed (9 for DC, 6 for RC, 7 for DN, and 10 for CT melanomas). A total of 10 slices of 10 μM per patient were employed, and only tumoral area was collected. cDNA was prepared using the High-Capacity cDNA Reverse Transcription kit (Applied Biosystem, Foster City, CA), and real-time PCR was performed using the DyNamo SYBR Green qPCR kit (Thermo Fisher Scientific), as previously reported (Quadri et al., 2021, 2022). Gene primers sequences are listed in Supplementary Table S1.

Transcriptomic analysis of RCM melanoma subtypes was performed at PharmaDiagen (Pordenone, Italy) using the nCounter Nanostring technology platform. In detail, the PanCancer Progression Panel (https://www.nanostring.com/products/ncounter-assays-panels/oncology/pancancer-progression/) was applied. This panel performs multiplex gene expression analysis with 770 genes involved in each step of the cancer progression, including angiogenesis, extracellular matrix remodeling, epithelial to mesenchymal transition, and metastasis.

Data were normalized by a unique housekeeping gene. Gene expression clustering analysis was performed on the

normalized gene means by Heatmapper (Babicki et al., 2016) using the Pearson distance measurement method.

To evaluate the differences in the gene expression profile among the RCM subtypes, paired comparisons were performed (RC vs. DC, CT vs. DC, DN vs. DC, RC vs. CT, and CT vs. DN melanomas), and gene fold changes were measured. For each comparison, the most significantly modulated genes were determined by fold change of ±1.5 and $P < 0.05$ (cut-off count > 30; coefficient of variation < 1). Gene Ontology (GO) biological process (BP) term enrichment was determined by DAVID functional annotation tools (https://david.ncifcrf.gov) through the upload of the differentially expressed genes (fold change of ±1.5, $P < 0.05$) for each comparison. The most significant GO BP terms ($P < 0.05$) were selected, and gene lists were generated. To provide a comprehensive view of the transcriptional profile, heatmaps including genes related to a specific GO BP (hydrolase and extracellular matrix, cell adhesion, angiogenesis, inflammation mediated by chemokine and cytokine signaling pathway, and cancer-associated transcription factors) were generated using the normalized gene expression means.

The differentially upregulated and downregulated gene (fold change of ±1.5, count cut-off > 30) in each comparison were uploaded onto Venny 2.1 (http://bioinfogp.cnb.csic.es/tools/venny) to generate a Venny diagram with unique and common genes for each group. Volcano plots, indicating $\log_2$ (fold change) versus $\log_{10}$ (*P*-value), was generated by Prism 9 (GraphPad Software, La Jolla, CA) to identify the most relevant genes, modulated into each comparison (RC vs. DC, CT vs. DC, DN vs. DC, RC vs. CT, RC vs. DN, and CT vs. DN melanomas). Subsequently, gene lists were analyzed by DAVID functional annotation tools, and the top 10 (five for RC vs. DC melanomas comparison) GO BP terms were represented by heatmap for each comparison and ranked by $-\log_{10}$ (*P*-value) (Prism 9, GraphPad Software). Finally, the GO BP terms representative of the Nanostring Panel (angiogenesis, extracellular matrix organization, inflammation, and cell adhesion) were defined for each comparison ranked by $-\log_{10}$ (*P*-value) by Heatmapper (Babicki et al., 2016) using Euclidean distance measurement method.

Melanoma skin reconstructs

For dermal reconstructs, 0.5 ml of a cell-free collagen solution (1.35 mg/ml rat tail type I collagen in DMEM with 10% fetal bovine serum and 1% penicillin/streptomycin) was added to tissue culture inserts (Transwell, Costar, Cambridge, MA) in 12-well plates. This precoated layer was overlaid with 1 ml of fibroblasts mixed with collagen type I solution (15×10^4 /ml). In the case of DN melanoma, spheroids were implanted in the dermal equivalent, and after 4 days of incubation at 37 °C, primary human keratinocytes (25×10^4 cells) were seeded on it to form epidermal equivalent. As a concern for CT melanoma, human keratinocytes and CT melanoma cells (5×10^4 cells) were seeded together on dermal reconstructs. Finally, skin reconstructs were exposed to the air, and the medium was changed every 2 days. After either 6 or 12 days, skin reconstructs were fixed with formalin for 2 hours at room temperature, dehydrated, and embedded in paraffin. Skin equivalent H&E staining, immunohistochemistry, and immunofluorescence were performed as previously reported (Quadri et al., 2021). Antibody dilutions are reported in Supplementary Table S2.

Statistical analysis

For clinical data (Table 1), statistical analysis was performed using STATA software, version 14 (Stata Statistical Software: release 14, StataCorp, College Station, TX). Descriptive statistics were presented for baseline demographic clinical characteristics for the entire group. Means and SDs were calculated for normally distributed data, whereas medians and first and third quartiles were calculated for data that were not normally distributed. Continuous variables were presented as the number of patients (n), mean, SD, minimum, and maximum and compared between subgroups using unpaired Student's *t*-test for two groups, whereas categorical variables were presented as frequency (n, percentage [%]) and compared using Pearson's chi-square test. $P < 0.05$ was considered statistically significant. For other data, the results are presented as mean ± SD or SEM from three independent experiments. Statistical analysis was performed with two-way ANOVA and Student's *t*-test using GraphPad Prism 9 (GraphPad Software). Significant *P*-values are indicated as follows: *$0.01 < P < 0.5$, **$0.001 < P < 0.01$, and ***$P < 0.001$.

SUPPLEMENTARY REFERENCES

Babicki S, Arndt D, Marcu A, Liang Y, Grant JR, Maciejewski A, et al. Heatmapper: web-enabled heat mapping for all. Nucleic Acids Res 2016;44:W147–53.

Pellacani G, De Pace B, Reggiani C, Cesinaro AM, Argenziano G, Zalaudek I, et al. Distinct melanoma types based on reflectance confocal microscopy. Exp Dermatol 2014;23:414–8.

Pellacani G, Guitera P, Longo C, Avramidis M, Seidenari S, Menzies S. The impact of in vivo reflectance confocal microscopy for the diagnostic accuracy of melanoma and equivocal melanocytic lesions. J Invest Dermatol 2007;127:2759–65.

Quadri M, Comitato A, Palazzo E, Tiso N, Rentsch A, Pellacani G, et al. Activation of cGMP-dependent protein kinase restricts melanoma growth and invasion by interfering with the EGF/EGFR pathway. J Invest Dermatol 2022;142:201–11.

Rajadhyaksha M, Grossman M, Esterowitz D, Webb RH, Anderson RR. In vivo confocal scanning laser microscopy of human skin: melanin provides strong contrast. J Invest Dermatol 1995;104:946–52.

Saltari A, Truzzi F, Quadri M, Lotti R, Palazzo E, Grisendi G, et al. CD271 downregulation promotes melanoma progression and invasion in three-dimensional models and in zebrafish. J Invest Dermatol 2016;136:2049–58.

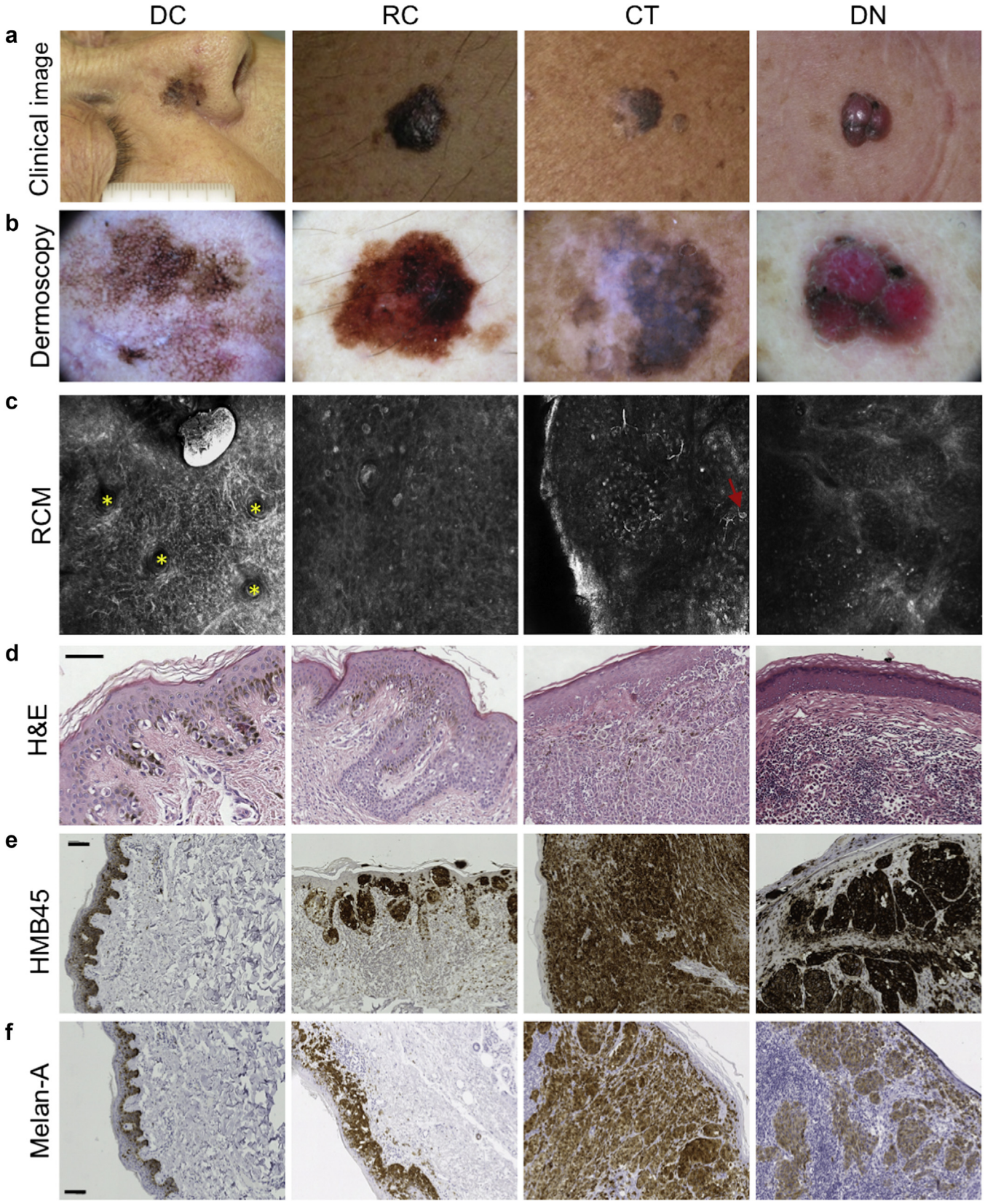

Supplementary Figure S1. Representative clinical, histopathological, and RCM images of melanoma subtype. (**a, b**) Clinical and dermoscopic image of RCM melanoma subtypes. (**c**) RCM image of RCM melanoma subtypes. DC: melanoma in the transition from the epidermis to DEJ shows numerous lines corresponding to melanoma cells with a dendritic shape (red arrow) coming out of the hair follicles (asterisk). RC: RCM shows the presence of several roundish large melanocytes (red arrows) with bright cytoplasm and hyporeflective nucleus. CT: RCM shows the presence of melanoma cells with dendritic shape, roundish cells (red arrows), and polymorphic cells (green arrow) within the dermal papilla. DN: RCM shows the presence of a cerebriform nesting (red arrows) located at the dermal level. (**d–f**) H&E, HMB45, and melan-A staining in each melanoma subtype. Bar = 50 μm. Melanoma biopsies and images were collected

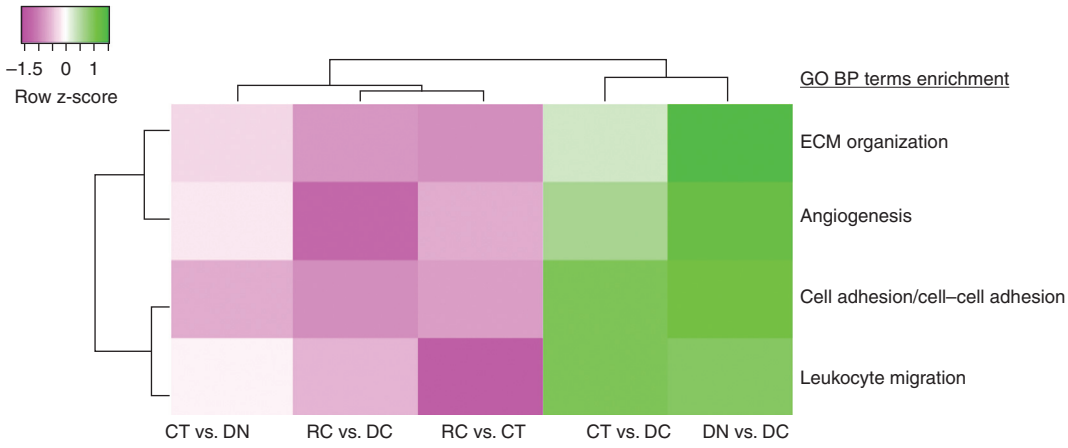

Supplementary Figure S2. Cluster analysis. Cluster analysis representing the main representative GO BP terms for each comparison ranked by $-\log_{10}$ (*P*-value). BP, biological process; CT, combined-type; DC, dendritic cell; DN, dermal nest; ECM, extracellular matrix; GO, Gene Ontology; RC, round cell.

after patients provided informed written consent approved by the Ethical Committee of Area Vasta Emilia Nord (protocol number 475, Doc. 118/2014 − 09/02/2016). CT, combined-type; DC, dendritic cell; DEJ, dermal–epidermal junction; DN, dermal nest; RC, round cell; RCM, reflectance confocal microscopy.

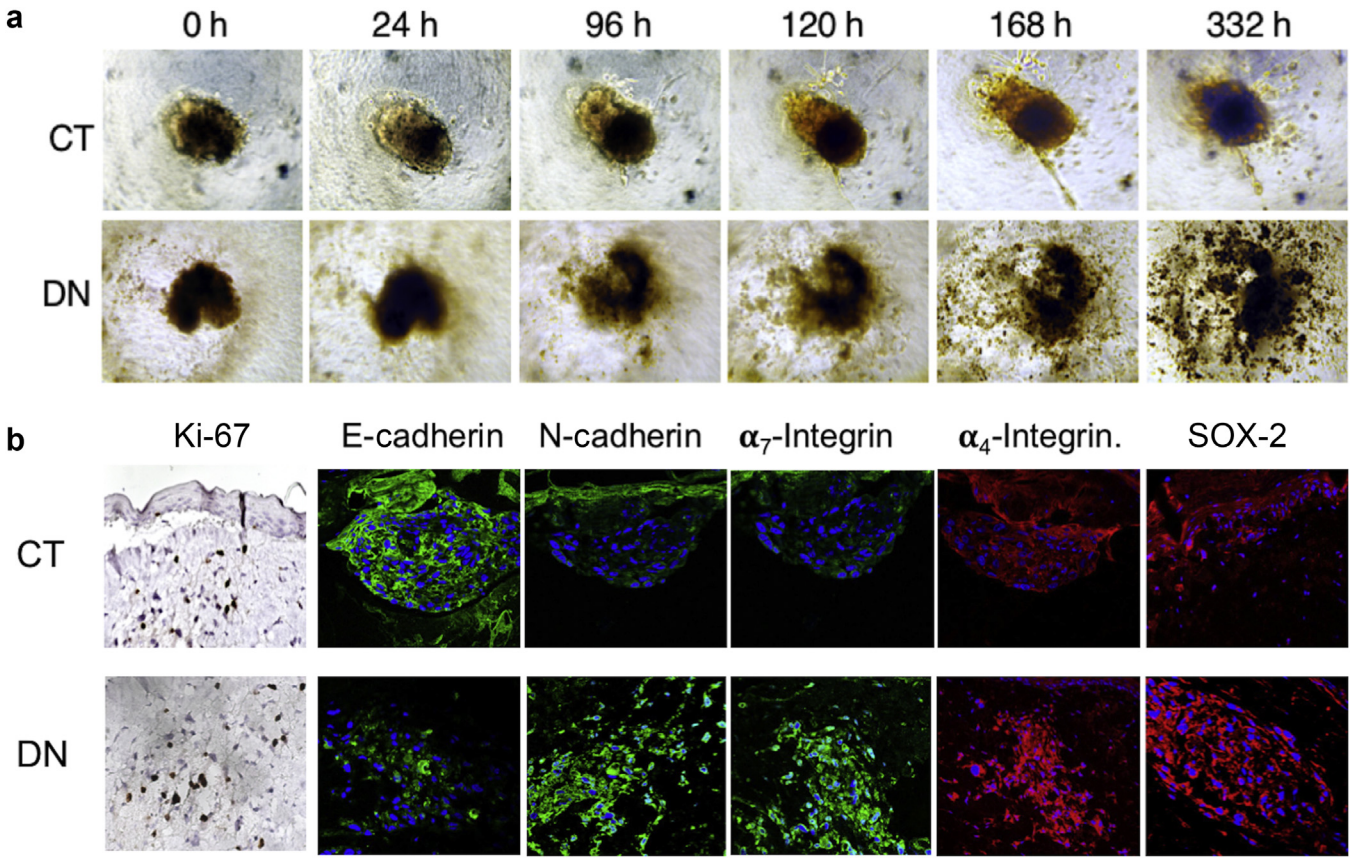

Supplementary Figure S3. Collagen invasion assay and skin reconstruct of the most aggressive RCM subtypes. (**a**) CT and DN melanoma biopsies were digested, and cells were seeded in hanging drop culture to obtain spheroids. At 72 h after seeding, spheroids were transferred in a type I collagen matrix, and pictures were taken from 0 to 332 h. (**b**) Melanoma skin equivalents were performed using cells derived from CT and DN melanoma. After 14 days of emersion conditions, melanoma skin equivalents were paraffin-embedded. The expression of MIB/Ki-67 was evaluated by immunohistochemistry. E- and N-cadherin, α_7 integrin, α_4 integrin, and SOX-2 expression were evaluated by immunofluorescence. CT, combined-type; DN, dermal nest; h, hour; RCM, reflectance confocal microscopy.

Supplementary Table S1. Primers for Real-Time PCR

Gene	Forward Primer (5′ to 3′)	Reverse Primer(5′ to 3′)
β-actin	TGGATGATGATATCGCCGCGCTCG	CACATAGGAATCCTTCTGACCCA
NGFR	TGAGTGCTGCAAAGCCTGCAA	TCTCATCCTGGTAGTAGCCGT
BIRC5	GCATGGGTGCCCCGACGTTG	GCTCCGGCCAGAGGCCTCAA
CXCL8	GAATGGGTTTGCTAGAATGTGATA	CAGACTAGGGTTGCCAGATTTAAC

Supplementary Table S2. List of Primary Antibodies Used in the Study

Antibody	Provider	Dilution	Application
HMB45	Ventana, Roche (Rotkreuz, Switzerland)	Ready to use	IHC
Melan-A	Ventana, Roche	Ready to use	IHC
$BRAF^{V600E}$	Ventana, Roche	Ready to use	IHC
Ki-67	Dako, Agilent (Santa Clara, CA)	1:200	IHC
MERTK	MilliporeSigma, (Burlington, MS)	1:100	IHC
NESTIN	Arigo Biolaboratories (Hsinchu City, Taiwan)	1:100	IHC
HIF1α	Novus Biologicals (Centennial, CO)	1:50	IHC
ABCB5	Novus Biologicals	1:100	IHC
SOX-10	Novus Biologicals	1:200	IHC
SOX-2	Novus Biological	1:200	IHC/IF
CD133	Biorbyt (St. Louis, MO)	1:100	IHC
CD271	MilliporeSigma	1:100	IHC
E-cadherin	BD Biosciences (Franklin Lakes, NJ)	1:100	IHC/IF
		1:1,000	WB
N-cadherin	BD Biosciences	1:100	IHC/IF
		1:1,000	WB
α7 integrin	Santa Cruz Biotechnology (Dallas, TX)	1:100	IHC/IF
		1:1,000	WB
α4 integrin	Santa Cruz Biotechnology	1:100	IHC/IF
		1:1,000	WB

Abbreviations: IF, immunofluorescence; IHC, immunohistochemistry; WB, western blot.